Journal of Solid State Chemistry 184 (2011) 1834–1842

Contents lists available at ScienceDirect

Journal of Solid State Chemistry

journal homepage: www.elsevier.com/locate/jssc

Phase relations in a barium-rich high-temperature region (25–45 mol% CuO, 900–1100 °C) of the $BaO–CuO_x$ system

L.A. Klinkova [a], V.I. Nikolaichik [b,*], N.V. Barkovskii [a], V.K. Fedotov [a]

[a] Institute of Solid State Physics of the RAS, Chernogolovka, Moscow District, 142432, Russia
[b] Institute of Microelectronics Technology of the RAS, Chernogolovka, Moscow District, 142432, Russia

ARTICLE INFO

Article history:
Received 30 October 2010
Received in revised form
19 May 2011
Accepted 20 May 2011
Available online 30 May 2011

Keywords:
Phase diagram
$BaO–CuO_x$ system
XRD
Transmission electron microscopy
Iodometric titration

ABSTRACT

The phase relations have been studied in the $BaO–CuO_x$ system in the range of 25.0–45.0 mol% CuO at 900–1100 °C at $P(O_2)=21$ kPa (air) by visual polythermal analysis (VPA), powder X-ray diffraction (XRD), electron diffraction (ED) with simultaneous energy-dispersive X-ray (EDX) elemental analysis in a transmission electron microscope (TEM), and iodometric chemical analysis. The discrete deviations 2.02 (101:50), 2.04 (102:50), 2.10 (105:50) of Ba/Cu (Ba:Cu) composition from the stoichiometric ratio 2:1 have been found for the known $Ba_2CuO_{3+\delta}$ oxides in the subsolidus region 900–970 °C. Unit cell parameters of the 101:50 orthorhombic oxide, 102:50 tetragonal one, 105:50 orthorhombic one are, respectively, $a=4.049$, $b=3.899$, $c=13.034$ Å; $a=3.985$, $c=12.968$ Å; $a=4.087$, $b=3.897$ and $c=12.950$ Å. ED patterns of the 101:50, 102:50, 105:50 oxides show characteristic supercell reflections with the respective vector 1/60[5 4 0], $\approx 2/11\langle 1\,1\,0\rangle$ and 1/6[2 0 0]. Oxides of the 2:1, 7:4, 5:3 and 23:20 compositions have been found in the crystallization region 970–1050 °C. Unit cell parameters of the 2:1 orthorhombic oxide are $a=4.095$, $b=3.795$, $c=13.165$ Å. Interplanar spacings and X-ray characteristic peak intensities of the 7:4, 5:3 and 23:20 oxides are given. Oxides 2:1 and 7:4 melt pseudocongruently at 1020 and 1005 °C, oxides 5:3 and 23:20 melt incongruently at 995 and 980 °C, respectively. A diagram of the phase relations in the studied region of the $BaO–CuO_x$ system has been constructed, whose structure is considered as the total projection of phase states of the system existing for different x.

1. Introduction

The $BaO–CuO_x$ system is of interest due to its inherent linkage with the Y–Ba–Cu–O system. The knowledge of the phase diagram of the latter system involves understanding the phase relations in the $BaO–CuO_x$ system. Literature data about oxides in the $BaO–BaCuO_2$ range are given in Table 1. Oxides of the cation compositions (Ba:Cu) 3:1 [1,2], 2:1 [2–7] and 1:1 [8,9] have been reported. It is believed that three modifications (two orthorhombic and one tetragonal) of the 2:1 oxide differ in oxygen content [2]. The 1:1 ($BaCuO_2$) oxide has a cubic cluster structure [9,10], its X-ray diffraction pattern looks the same at variation of cation ratio (Ba/Cu) in the range of 0.87–1.10 [9,11,12]. Different variants of phase diagrams of the $BaO–CuO_x$ system in the $BaO–BaCuO_2$ (barium-rich) range (Fig. 1) were published [7,13–18], which vary in the presence of eutectics and its composition, and in the existing oxides as well.

The inconsistence of the data about the phase diagram of $BaO–CuO_x$ system necessitates a more thorough investigation. In the work we studied the 25–45 mol% CuO region at 900–1100 °C with use of a complex approach developed in our studies of the K–Ba–Bi–O superconducting system and its parent Ba–Bi–O system [19], when the technique of analytical transmission electron microscopy has been systematically used along with usual methods employed for studying phase relations in metal-oxide systems (physical–chemical methods, electron probe microanalyses, and XRD) that made it possible to discover a large number of discrete oxides with ordered structures.

2. Materials and methods

The starting materials were analytical purity BaO_2 (97 wt%) and high purity CuO (99.99 wt%). Mixtures of specified composition with a step of 1 mol% CuO were homogenized and pressed into pellets, which were baked in alumina crucibles in air (oxygen partial pressure $P(O_2)=21$ kPa). The samples were quenched on a cooled copper plate or by submersion into liquid nitrogen. After nitrogen quenching, crucibles with samples were evacuated to

* Corresponding author. Fax: +7 496 524 4225.
E-mail address: nikola@iptm.ru (V.I. Nikolaichik).

0022-4596/$ - see front matter © 2011 Elsevier Inc. All rights reserved.
doi:10.1016/j.jssc.2011.05.028

Table 1
Literature data on synthesis conditions and unit cell parameters of barium-rich oxides of the $BaO–BaCuO_2$ system.

No.	Oxide	Synthesis conditions				Unit cell parameters (Å)			Ref.
		Reagents	Atm.	T (°C)	τ (h)	a	b	c	
1	Ba_3CuO_4	BaO, CuO	Air	905→20	12				[1]
2	Ba_3CuO_4	$Ba(NO_3)_2$, Cu_2O	Ar	860	24	7.883		15.55	[2]
3	Ba_2CuO_3	$Ba(NO_3)_2$, Cu_2O	Air Ar	900 860	24	4.107	3.780	13.140	[2]
4	$Ba_2CuO_{3+\delta}$	$Ba(NO_3)_2$, Cu_2O	Air Vac.	900 600	4	4.096	3.909	12.959	[2]
5	$Ba_2CuO_{3+\delta}$	$Ba(NO_3)_2$, Cu_2O	Air Vac.	900 900	4	3.992		12.985	[2]
6	$Ba_2CuO_{3.3}$	BaO_2, CuO	O_2	900→20		4.0969	3.9038	12.9441	[3]
7	Ba_2CuO_3	BaO_2, CuO	O_2	580→20 750→20 800	17 19 22	12.9655	4.1007	3.9069	[4]
8	$Ba_2CuO_{3+\delta}$	BaO_2, CuO	O_2	800–880	100	4.093	3.906	12.949	[5]
9	$Ba_2CuO_{3.3}$	BaO_2, CuO	Air	830→20	48	4.0959	3.9047	12.9420	[6]
10	$Ba_2CuO_{3.088}$	CuO, BaO_2	Air	830	48	3.9923		12.9686	[6]
11	Ba_2CuO_3	BaO_2, CuO	Air	830→20	48	12.9655	4.1007	3.9060	[7]
12	Ba_2CuO_3	BaO_2, CuO	Air	830	48	12.975		3.992	[7]
13	$BaCuO_2$	BaO, $BaCO_3$, CuO	Air	850	48	18.322			[8]
14	$BaCuO_2$	BaO_2, CuO	Air Vac.	800 800	20 20	18.26			[9]

remove the condensed moisture. X-ray diffraction patterns were taken under a vaseline layer in a Siemens D-500 diffractometer with a monochromator in Cu$K\alpha_1$ radiation. Cell parameters were determined by a profile analysis with an error ± 0.006 Å.

The composition and structure were analyzed in a JEM-2000FX TEM equipped with an Oxford Instruments X-ray energy-dispersion system. A procedure of sample preparation for TEM studies included material grinding in an agate pestle under hexane protection, ultrasonic agitation and dripping hexane suspension onto clean Be-grids or Be-grids with supporting carbon films. The first variant was used when carbon content of the oxides was evaluated. As X-ray spectra in a TEM show scattering of element peaks ratio for different particles even for a phase of the rigid composition (mainly due to varied orientation of particles relative to incident electron beam), we obtained X-ray spectra from many particles displaying the same characteristic electron diffraction pattern and calculated the average Ba/Cu composition. Integer Ba:Cu ratio were selected as minimal to be close to the experimental average compositions. This statistical approach to assign the element compositions for the phases has been found to secure a high precision.

The average oxidation state of copper in samples was calculated from the chemical analysis data obtained via procedures evaluating the content of copper ions in different oxidation state ($+1$, $+2$, $+3$) by iodometric titration [20].

Infrared spectra were measured for samples crushed under vaseline using a Carl Zeiss UR-20 spectrometer.

Two major problems were met to prepare samples. The first one was related with barium–copper oxides that are highly susceptible to hydrolysis which was also noted in [2,6]. Hydrolysis takes place both during air and liquid nitrogen quenching, and possibly at X-ray profiling despite the presence of a protective vaseline layer. The product of hydrolysis is $Ba_2[Cu(OH)_6]$ identified according to [21]. It was noted in our electron diffraction studies that $Ba_2[Cu(OH)_6]$ is highly sensitive to electron irradiation in comparison with oxides of the Ba–Cu–O system so that its structure was quickly destroyed under electron beam.

The second problem is simultaneous synthesis of several oxides in one sample at any temperature above 900 °C. In the subsolidus region, microinhomogeneities existing in samples provide conditions for joint crystallization of phases, which are only slightly different in cation composition. In crystallization region, there is an additional condition related with a complex mechanism of melting that leads to formation of the $BaCu_2O_2$ oxide in the melt.

3. Results

3.1. Visual polythermal analysis

Samples for VPA were baked consequently at 720 (during 2 h), 750 (1 h), 850 (0.5 h), 880 °C (0.5 h) and then in steps of 10 °C (0.5 h) up to melting. Temperature and time of baking were selected to optimize the process when conditions of the complete synthesis, the absence of $BaCO_3$ formation, avoiding of a long contact between the melt and the crucible material are achieved.

The next phenomena were observed at baking the pellets. At the beginning, a pellet volume was decreased due to agglomeration and oxygen loss. Then traces of liquid of an unknown nature were noticed at the bottom of crucible. Traces were usually retained with further baking. On further temperature rising, a pellet started to stick to the crucible bottom, this moment was assumed as the start of melting and the transition into a liquid+solid (L+S) state. The final stage of the complete melting (L state) was detected when a mobile melt and a smooth surface were observed at quenching. It was noticed that with increasing barium content in samples the melt went up the walls of a crucible. This circumstance reduced the accuracy in determining

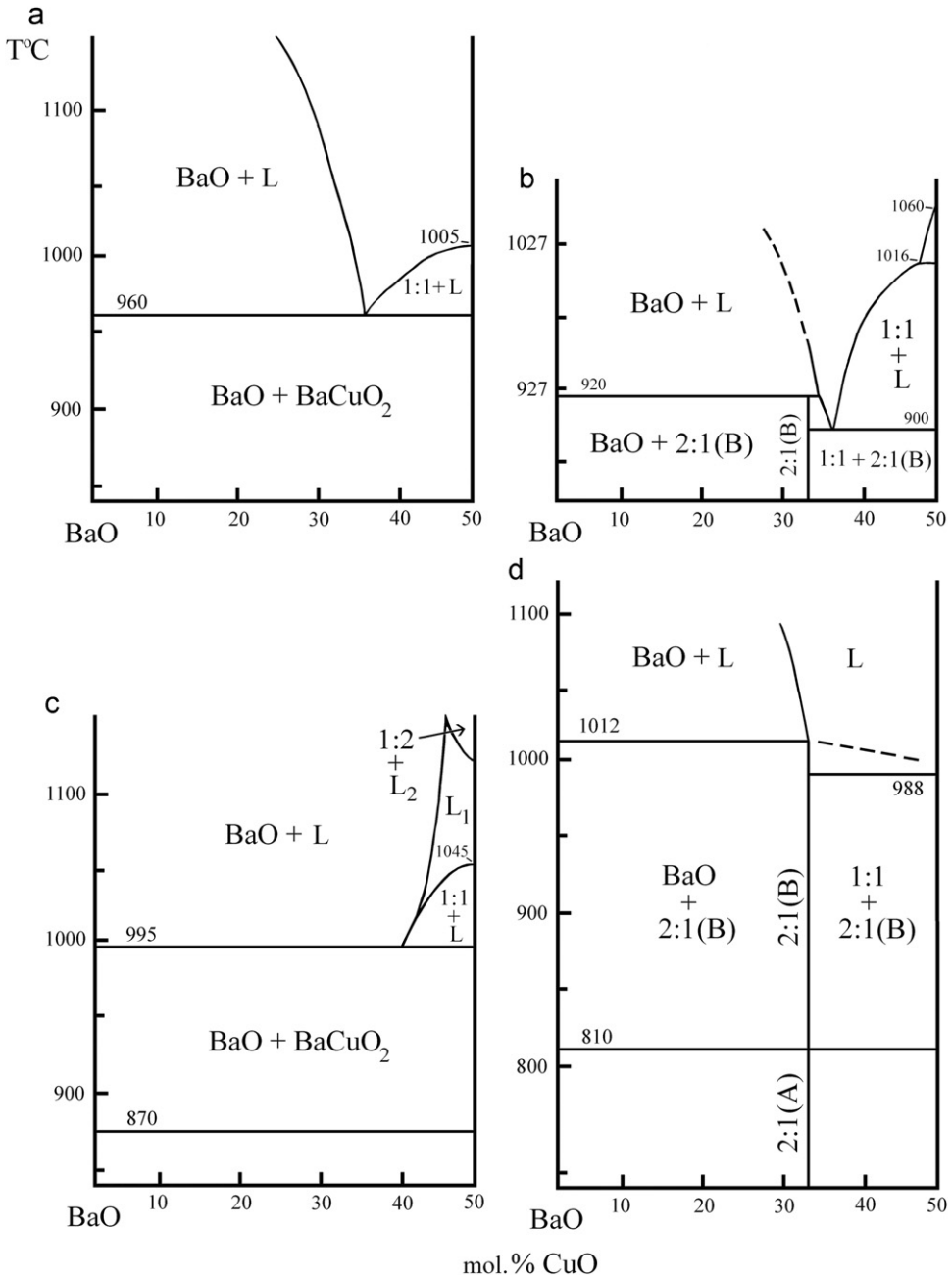

Fig. 1. Variants of phase diagrams of the BaO–CuO_x system in the barium-rich range presented in the literature. (a) [13], (b) [7], (c) [15] and (d) [17].

the liquidus temperature, but we estimated that an error did not exceed ± 5 °C.

Fig. 2 shows the crystallization and liquidus region of the phase diagram of the BaO–CuO_x system in the range of 25.0–45.0 mol% CuO at 950–1100 °C at $P(O_2)=21$ kPa constructed on the basis of VPA data (VPA diagram) by studying 21 samples. The liquidus line has been determined by temperature of the complete melting. The temperature of the solidus line, when indications of sample submelting in the range of 31.0–45.0 mol% CuO appear, is estimated as 970 °C. This temperature is only conditionally can be taken as eutectic, since none of the samples melted in one stage. Melting of $\approx$33.3 and 37.0 mol% CuO compositions at 1020 and 1010 °C respective temperature can be attributed to the process of congruent melting of individual phases. There are fields in the crystallization region, which are formed by phases melting incongruently.

3.2. Powder X-ray diffraction and electron diffraction with elemental analysis

3.2.1. Subsolidus region (900–970 °C)

Three oxides of the close compositions (Ba:Cu) 101:50, 102:50 and 105:50 near to the 2:1 ratio have been found in the subsolidus region (900–970 °C). They are of the related structures, which is evidenced by a similar view of XRD and ED patterns (the reflection conditions $h+k+l=2n$), with a basic crystallographic motive of their structures formed of a layered stacking of double barium and single copper planes in the [0 0 1] direction [2].

The 101:50 oxide coexists with the 102:50 and 105:50 oxides in the 25.0 and 33.0 mol% CuO samples. In the 34.5 mol% CuO sample, it coexists with an oxide having a cubic structure similar to that of the $BaCuO_2$ oxide but enriched in copper. The 101:50 oxide has an orthorhombic lattice with unit cell parameters (without regard for

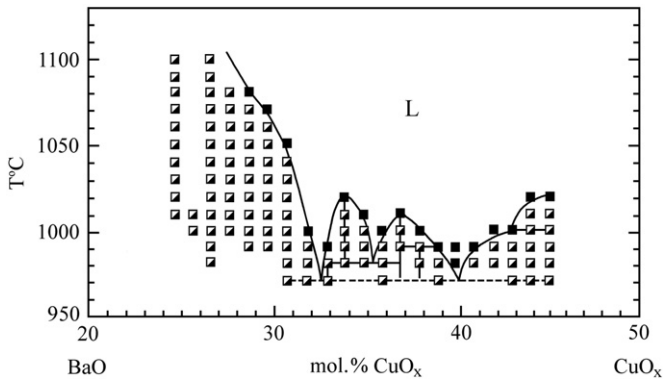

Fig. 2. Crystallization and liquidus region of phase diagram of the $BaO–CuO_x$ system in the range of 25.0–45.0 mol% CuO at $P(O_2)=21$ kPa (air) constructed on the basis of data of visual polythermal analysis. Half-filled squares correspond to a liquid+solid (L+S) state, filled squares correspond to a liquid (L) state.

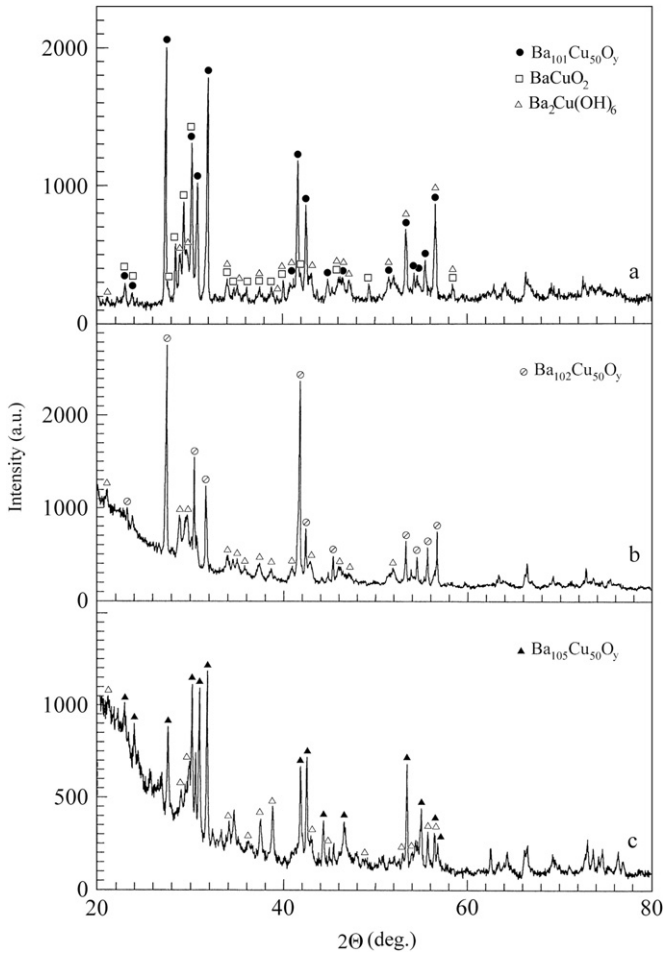

Fig. 3. XRD patterns of the 34.5 (a) and the 29 mol% CuO sample (b,c) baked at 900 °C for 2 h (a,b) and (2+2) h with an intermediate homogenization (c). The samples contain the dominant phases 101:50 (a), 102:50 (b) and 105:50 (c).

supercell reflections) $a=4.049$, $b=3.899$ and $c=13.034$ Å (Fig. 3a) close to those of the $Ba_2CuO_{3+\delta}$ and $Ba_2CuO_{3.3}$ oxides (Nos. 4 and 9, Table 1). The characteristic ED pattern of the 101:50 oxide (Fig. 4a) shows supercell reflections with the vector $\mathbf{q}=1/60[5\,4\,0]$ of very small length.

The oxide of the composition (Ba:Cu) 102:50 is formed in a sample with the content of 29.0 mol% CuO at the short-term (2 h) annealing at 900 °C (Fig. 3b). This oxide crystallizes in a tetragonal lattice with unit cell parameters $a=3.985$ and $c=12.968$ Å. The characteristic ED pattern (Fig. 4b) in the [0 0 1] zone axis, which is of the four-order symmetry consistent with the tetragonal structure of the oxide, shows supercell reflections along the ⟨1 1 0⟩ directions with the incommensurate vector $\mathbf{q}\approx 2/11$ ⟨1 1 0⟩ in addition to the main reflections from the basic unit cell. In terms of close unit cell parameters, the 102:50 oxide is related to the $Ba_2CuO_{3.088}$ oxide (No. 10, Table 1).

The 105:50 oxide is formed after additional homogenization and second annealing of the 29.0 mol% CuO sample (Fig. 3c). Its crystal lattice is of orthorhombic symmetry with unit cell parameters $a=4.087$, $b=3.897$ and $c=12.950$ Å close to those of the Ba_2CuO_3 oxide (No. 7, Table 1). The corresponding ED pattern (Fig. 4c) shows two-fold symmetry consistent with an orthorhombic lattice. Supercell reflections with the vector $\mathbf{q}=1/6$ [2 0 0] and large splitting of diffractions spots are observed, which points to the presence of twin domains with the twin boundary $(1\,\bar{1}\,0)$ in the structure.

Elemental analysis data for oxide particles displaying the characteristic ED patterns are presented in Fig. 5. The integer ratio (Ba:Cu) 101:50, 102:50 and 105:50 correspond to the averaged values (Ba/Cu) 2.02, 2.04 and 2.10, respectively.

3.2.2. Crystallization and liquidus region (970–1100 °C)

Four oxides 2:1, 7:4, 5:3 and 23:20 of different structures have been found in this region.

The 2:1 oxide melts pseudocongruently at 1020 °C, which means that the composition of melt is different from that of oxide. The 7:4 oxide melts pseudocongruently also at 1005 °C and forms an eutectics (≈990 °C, 34.5 mol% CuO) with the 2:1 oxide. The 5:3 oxide melts incongruently at 995 °C and forms an eutectics (≈970 °C, 42.0 mol% CuO) with the 23:20 oxide. The 23:20 oxide melts incongruently at 980 °C.

Fig. 6 shows X-ray patterns of the samples with peaks characteristic of 2:1, 7:4, 5:3 and 23:20 phases. An X-ray pattern of the 2:1 oxide evidences that its structure is of orthorhombic symmetry with the unit cell parameters $a=4.095$, $b=3.795$, $c=13.165$ Å, its structure is similar to that of the Ba_2CuO_3 oxide (No. 2, Table 1). Table 2 presents interplanar spacings and intensities of X-ray peaks characteristic of the 7:4, 5:3 and 23:20 oxides.

Observations of ED patterns of the 7:4 oxide have revealed the existence of the unique six-order symmetry axis (Fig. 7a and b) that points to its hexagonal or rhombohedral crystal lattice.

The 23:20 oxide has a tetragonal lattice as its ED patterns (Fig. 7c and d) display the unique four-order symmetry axis. Comparison of ED patterns of the 23:20 oxide with those of the cubic oxide $BaCuO_2$ [10] discloses their similarity in several zone axes that indicates a relationship between their structures. The structure of the 23:20 oxide can be considered as a derivative of that of the $BaCuO_2$ oxide with lowering symmetry from cubic to tetragonal.

All samples quenched at temperature corresponding to the crystallization and liquidus region contain the oxide $BaCu_2O_2$. Particles of an oxide of the composition 11:10 displaying ED patterns similar to those of the 23:20 oxide were found in the 42.0–45.0 mol% CuO samples quenched at 1000–1020 °C.

Ba-rich particles (their crystal structures were not possible to observe due to the decomposition) were found in the 25.0–32.0 mol% CuO samples, that suggests the existence of 11:5 and 3:1 oxides. The samples quenched at temperature higher 1050 °C contained barium aluminates $Ba_3Al_2O_6$ [22] and $Ba_7Al_2O_{10}$ [23], which indicates interaction of the crucible material (Al_2O_3) with the samples.

Fig. 8 presents a diagram of phase relations in the $BaO–CuO_x$ system in the range of 30.0–45.0 mol% CuO at 900–1050 °C

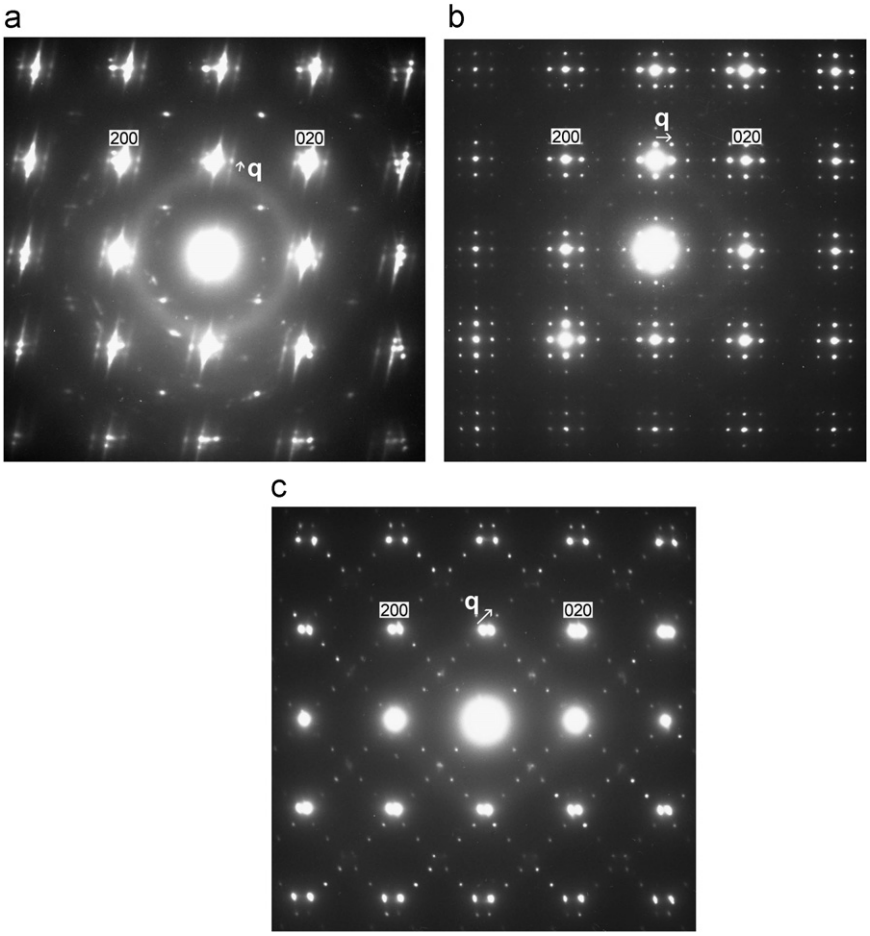

Fig. 4. ED patterns of the oxides 101:50 (a), 102:50 (b), 105:50 (c). Zone axis [0 0 1].

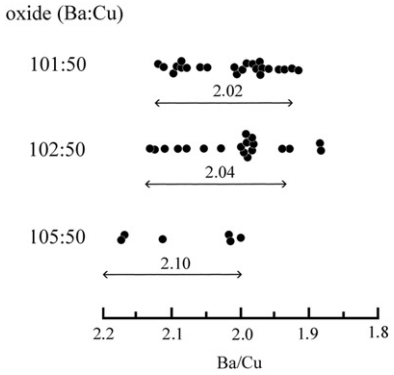

Fig. 5. Ba/Cu ratio data (the averaged values and intervals of standard deviation) measured in the TEM for particles displaying the characteristic ED patterns of the oxides.

constructed on the data obtained by VPA (the liquidus line), XRD and ED with elemental analysis.

3.3. Chemical analysis

Results of chemical analysis of the samples quenched at 950–1080 °C into liquid nitrogen are given in Table 3. It is seen that the average oxidation state of copper ($\overline{Cu}$) decreases with temperature rising. Copper ions in the oxidation state +3 exist in Ba-rich samples at temperature lower 970 °C inclusive. Above the eutectic temperature (970 °C) samples melt with the formation of $BaCu_2O_2$ (where all copper ions are in the oxidation state +1). With further heating up to the complete melting the 27.4–40.0 mol% CuO samples loose oxygen so that $\overline{Cu}$ decreases to 1.53–1.66. All the phases from the crystallization region appear to contain copper ions mainly in the oxidation state +2, as the presence of $BaCu_2O_2$ is substantial. The $\overline{Cu}$ value of 2.12 at 970 °C for the 34.6 mol% CuO composition rules out the presence of liquid indicating that this point of the phase diagram is in the subsolidus region.

Taking into account the chemical analysis data showing the change of oxygen content with variation of temperature and CuO content, the phase diagram in Fig. 8 should be considered as the total projection of phase states of the system existing at different x in CuO_x.

3.4. Formation of oxycarbonates

Literature data [24–30] (Table 4) report the existence of alkali-earth element(s)-copper oxycarbonates, which can be competitive phases, when synthesis is carried out under ambient atmospheric conditions.

In relation to this topic, we have measured infrared absorption spectra of 2:1 (33.3 mol% CuO) samples quenched at 950 and 1020 °C after short-time baking (1 and 0.5 h). The IR spectra (Fig. 9) do not show the complete set of absorption bands at 644.1, 871.7 and 1402.0 cm^{-1} characteristic of CO_3^{2-} ions, e.g. in $Ba_4CaCu_2CO_3O_{6+\delta}$ [30] or in $BaCO_3$ [31]. So the IR spectra do not support the noticeable presence of CO_3^{2-} ions in the synthesized samples.

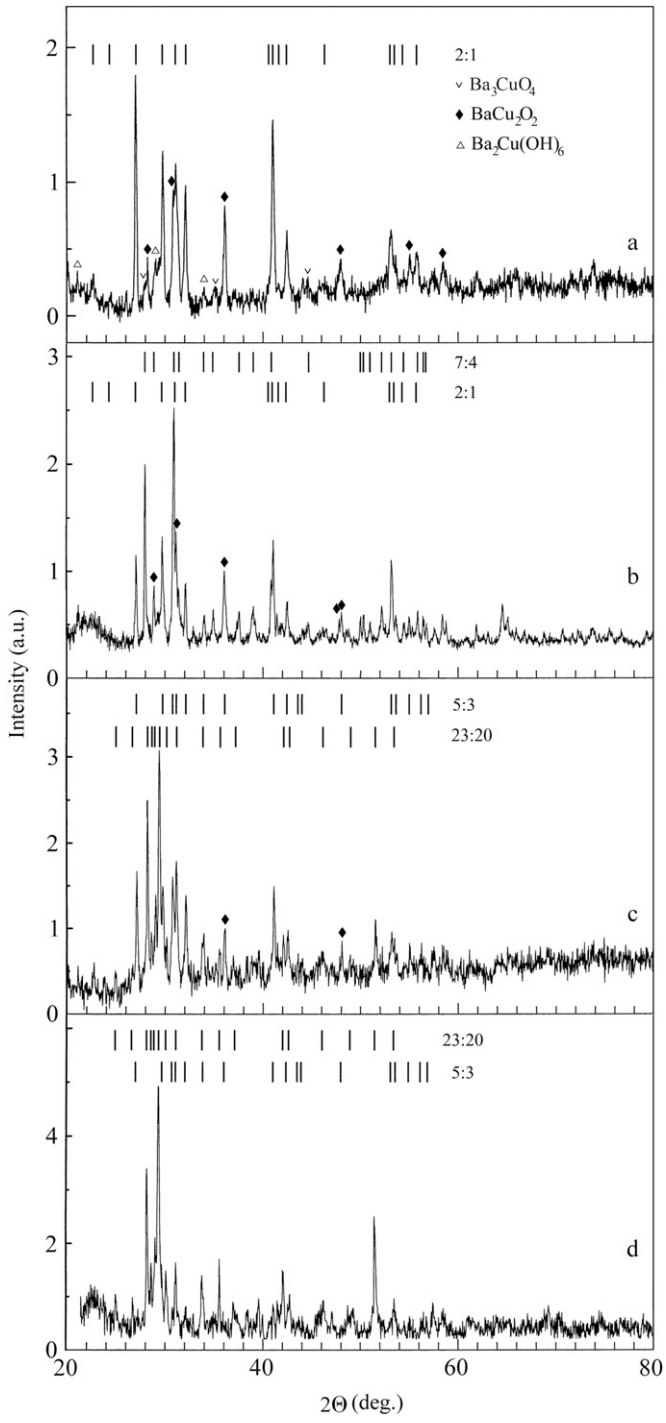

Fig. 6. XRD patterns (after background cancellation) of the 33.3 (a), 36.4 (b), 40.0 (c), 43.5 mol% CuO samples baked at 1020 (a), 1000 (b), 980 °C (c, d). Specific lines of the 2:1, 7:4, 5:3 and 23:20 oxides are marked off by bars.

XRD patterns of the synthesized samples (Figs. 3 and 6) do not contain the lines characteristic of the oxycarbonates with high content of alkali-earth elements ([27–30], Table 4). It means that the fraction of oxycarbonate phases in our samples is below the sensitivity of XRD technique (≤ 5 wt%).

Nevertheless, when studying synthesized samples in the electron microscope we have found particles, which are always analyzed at thin edge area, of the composition (Ba:Cu) 2:1 and 5:3 displaying ED patterns characteristic of oxycarbonates. ED patterns of 2:1 particles looks alike to those of oxycarbonate

Table 2
Interplanar spacings (d_{obs}, Å) and X-ray characteristic peak intensities I_{rel} (%) of the (Ba:Cu) oxides.

7:4		5:3		23:20	
d_{obs}	I_{rel}	d_{obs}	I_{rel}	d_{obs}	I_{rel}
3.176	98	3.281	100	3.551	13
3.078	32	2.991	74	3.334	10
2.876	100	2.894	93	3.153	60
2.833	23	2.860	73	3.105	34
2.559	16	2.776	33	3.075	30
2.382	17	2.631	37	3.026	100
2.297	30	2.479	50	2.955	25
2.198	9	2.188	91	2.858	22
2.020	13	2.122	43	2.638	25
1.820	13	2.070	20	2.512	17
1.809	10	2.051	17	2.408	3
1.787	18	1.889	33	2.138	18
1.749	39	1.720	33	2.110	14
1.718	12	1.705	17	1.963	7
1.681	16			1.856	8
1.642	13			1.771	40
1.626	7			1.711	8
1.620	6				

$BaSrCuO_{2.92}CO_3$ [28]. They fit to a primitive tetragonal lattice with unit cell parameters $a \approx 5.6$ and $c \approx 8.1$ Å, a structure motive of the unit cell can be imagined as two consecutive perovskite cells. EDX analysis reinforced the carbon presence, significant scattering of carbon content from particle to particle was observed. The average composition for 2:1 particles found in the 950 °C sample corresponds to the formula $Ba_2Cu(CO_2)_{0.30}O_{3.05}$ (9 at% of carbon relative to the sum of barium, cooper and carbon). The ED patterns of 5:3 particles look similar to those of 2:1 particles differing in the reflection conditions, they correspond to oxycarbonate $Ba_2Cu_{1.2}(CO_3)_{0.8}O_{2.4}$ [27]. The similarity of ED patterns of tetragonal lattice of 2:1 and 5:3 particles implies the same structure motive with related unit cell parameters.

4. Discussion

The group of three oxides 101:50, 102:50 and 105:50 found in the subsolidus region (25–45 mol% CuO, 900–970 °C) having the cation compositions close to Ba:Cu=2:1 can be associated with the phases $Ba_2CuO_{3+\delta}$ (Table 1), which were assumed to have the same cation composition 2:1 but differ in oxygen content. We have discovered at analytical electron diffraction studies that the phases are, in fact, have different compositions. They display supercell reflections in electron diffraction patterns, which was not expected in the literature data obtained by XRD. The existence of supercell reflections is likely related with composition deviation from the 2:1 ration and cation ordering. The four oxides 2:1, 7:4, 5:3 and 23:20 were found in the crystallization region.

The discovery of the new oxides makes the phase diagram of the BaO–CuO_x system to be of the different appearance than the previous ones (Fig. 1). We have established a change of copper valence state both in the subsolidus region and in the crystallization region and right in the melt as well with increasing temperature. In this connection the BaO–CuO_x system has to be considered as a ternary system, where four condensed phases can be in equilibrium. The constructed phase diagram (Fig. 8) presents projections of phase states existing at different x in CuO_x onto the temperature-composition plane and shows a complex phase equilibrium existing in the system under given experimental conditions.

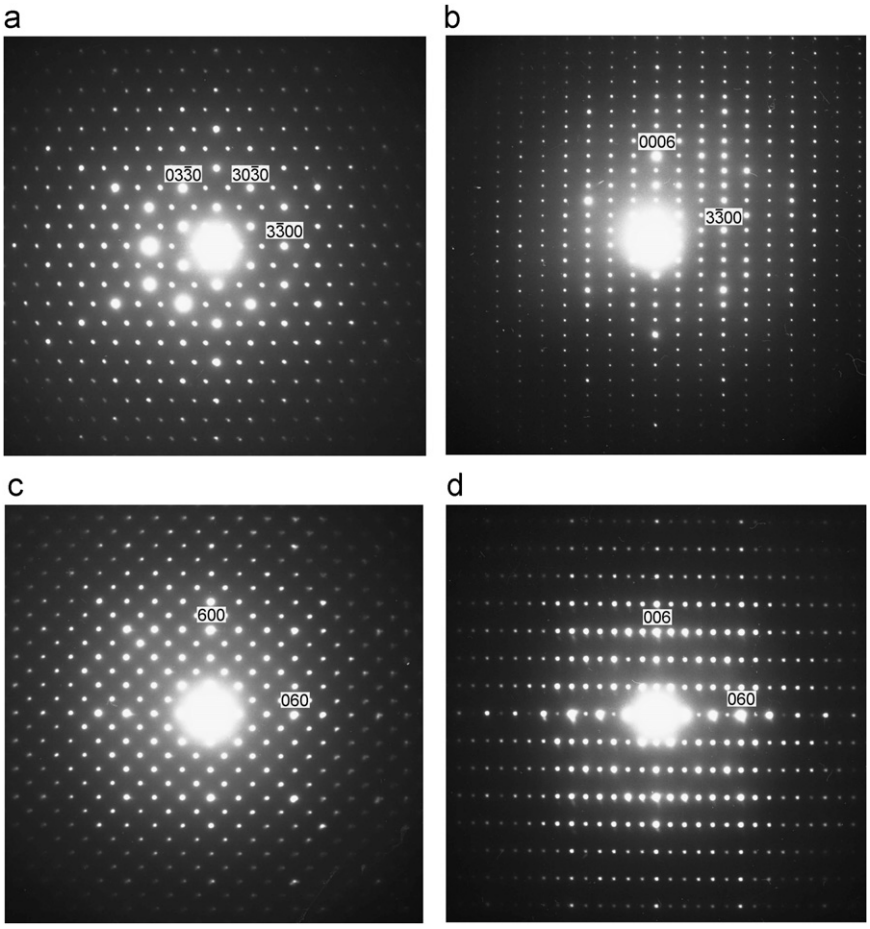

Fig. 7. ED patterns of the 7:4 (a,b) and 23:20 (c,d). Zone axis [0 0 0 1] (a), [1 1 $\bar{2}$ 0] (b), [0 0 1] (c), [1 0 0] (d).

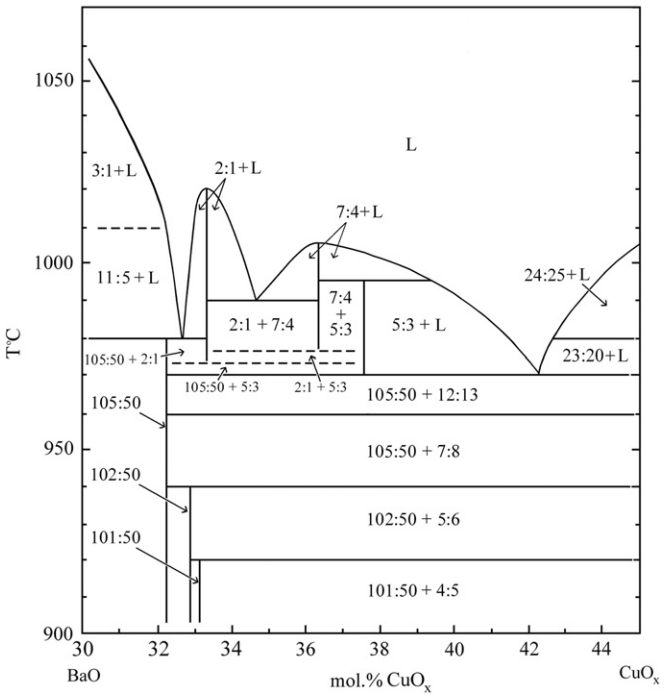

Fig. 8. A diagram of phase relations in the BaO–CuO_x system in the range of 30.0–45.0 mol% CuO at $P(O_2)$=21 kPa (air) constructed on the data obtained by VPA (the liquidus line), XRD, ED with elemental analysis and chemical analysis.

Table 3
Average oxidation state of copper ($\overline{Cu}$) in samples of barium–copper oxides quenched into liquid nitrogen (according to iodometric titration data).

No.	Synthesis conditions			Ion content (% of total copper ions)			$\overline{Cu}$
	CuO (mol%)	T (°C)	τ (h)	Cu^{+}	Cu^{2+}	Cu^{3+}	
1	27.4	1080	0.5	47.0	53.0	–	1.53
2	33.3	1020	0.5	37.8	62.2	–	1.62
3	36.4	1000[a]	1	34.5	65.5	–	1.66
4	40.0	1010	0.5	40.5	59.5	–	1.59
5	36.4	970[a]	1	–	87.7	12.3	2.12
6	33.3	950	1	–	82.8	17.2	2.17
7	34.5	950[b]	1	–	83.6	16.4	2.16
8	40.0	950	1	–	89.6	10.4	2.10

[a] Preliminary baking 900, 950 °C.
[b] Preliminary baking 900, 930 °C.

An important feature of the phase relations in the Ba-rich region of the BaO–CuO_x system is related with the melt. We have established that melting starts at 970 °C and results in formation of the $BaCu_2O_2$ oxide with copper in the oxidation state +1. In composition, this oxide refers to the Cu-rich region of the BaO–CuO_x system. In this connection, as melt composition does not correspond to that of at the points of melting of the 2:1 and 7:4 oxides, a mechanism of melting is pseudocongruent.

The presence of $BaCu_2O_2$ at melting (partial or full) is accounted for decomposition of oxides by reaching the temperature of their

Table 4
Literature data on synthesis conditions and unit cell parameters of alkali-element(s)-copper oxycarbonates.

Oxycarbonate	Synthesis conditions				Carbon content[a]	Unit cell parameters (Å)		Ref.
	Reagents	Atm.	T (°C)	τ (h)		a	c	
$BaCu_{1.15}O_{2.1}(CO_2)_{0.141}$ (Ba/Cu=0.87)	$BaCO_3$, CuO	CO_2	820–850 890–900	48 120	6[b]			[24]
$Ba_{0.9}CuO_{1.86}(CO_2)_{0.07}$	BaO_2, CuO	Ar	700	15	6.03[c] 3.6[d]	18.2394		[25]
$Ba_{0.9}CuO_{1.93}(CO_2)_{0.07}$	BaO_2, CuO	Ar	500	15	5.4[c] 3.6[d]	18.2334		[25]
$Ba_{0.9}CuO_{2.02}(CO_2)_{0.08}$	BaO_2, CuO	O_2	850	40	6.05[c] 4.04[d]	18.2597		[25]
$Ba_{44}Cu_{48}(CO_3)_6O_{87.9}$ (Ba/Cu=0.92)	$BaCO_3$, CuO	Air	850 850	24 24	6.1[c]	18.3069		[26]
$Ba_2Cu_{1.2}(CO_3)_{0.8}O_{2.4}$ (Ba/Cu=1.67)	$BaCO_3$, BaO_2, CuO	Air	700–950 1100	0.1–72 1/12	20[b]	3.990	8.073	[27]
$BaSrCuO_{2.92}CO_3$ ((Ba+Sr)/Cu=2.0)	$Ba(OH)_2 \cdot 8H_2O$ $SrCO_3$, CuO	O_2	820	60–70	25[d]	5.5899	7.7153	[28]
$Ba_4CaCu_{2.24}O_{6.96}(CO_3)_{0.5}$ ((Ba+Ca)/Cu=2.23)	$BaCO_3$, $CaCO_3$, CuO	Air (O_2)	950 1000	14 14	6.46[c]	5.799	7.992	[29]
$Ba_4CaCu_2O_{6+\delta}CO_3$ ((Ba+Ca)/Cu=2.5)	BaO_2, $CaCO_3$, CuO	Air	950 965	20 1	12.5[c]	5.7879	8.1409	[30]

[a] at% relative to the sum of Ba(Ca,Sr), Cu and C.
[b] Chemical analysis.
[c] Structure analysis.
[d] Thermogrametric analysis.

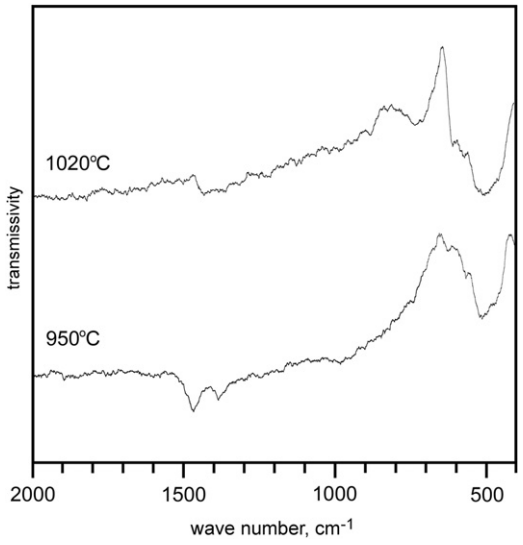

Fig. 9. Infrared spectra of the 33.3 mol% CuO samples quenched at 950 and 1020 °C into liquid nitrogen after 1 and 0.5 h baking, respectively.

thermal instability. A disproportionation of the oxide composition is accompanied by the formation, along with $BaCu_2O_2$ oxide, a barium-richer oxide. Such mechanism of melting provides the existence of several phases in quenched samples. Multi-phase nature of samples is retained under cooling because of access restrictions to the amount of oxygen in the presence of a hardened crust of the melt.

IR spectra and XRD patterns do not support the marked presence of barium–copper oxycarbonate phases in samples synthesized in our studies. Oxycarbonate phases are formed, when carbonates are used as starting reagents or long-term annealing in air is conducted. In this work BaO_2 as the starting reagent and short-term annealing were used. Earlier we have studied processes that takes place at annealing of BaO_2 in air [11]. It was found that oxygen loss takes place at 780–860 °C for 2 h, and then the sample starts to absorb CO_2 from air. BaO_2–CuO samples of the composition 3:2, 1:1, 2:3 and 1:2 behave in the same manner. A sharp mass loss at 850–900 °C was observed, it is slower above 900 °C. The obtained results show that the technique of short annealing makes it possible to avoid a marked occurrence of oxycarbonates. However, as it follows from our electron diffraction studies, when the thinnest part of a particle at the edge is only analyzed, CO_2 penetrates into surface area of the material leading to formation of oxycarbonates phases to a small extent. More studies are necessary to clarify at what stages (material synthesis or specimen preparation for analysis) carbonization takes place.

A structure analysis of the known oxycarbonates (Table 4) recognizes two structure types: the cubic one based on the $BaCuO_2$ structure and the tetragonal one. The first type includes oxycarbonates of the composition (Ba/Cu) 0.87 [24], 0.90 [25] and 0.92 [26]. They contain 3.6–6.05 at% carbon (relative to the sum of Ba, Cu and C) and can be considered as derivatives of matrix oxides (Ba:Cu) 7:8, 9:10 and 12:13 having the cubic $BaCuO_2$ structure and existing in the copper-rich region of the $BaO–CuO_x$ system [32]. The barium-rich oxycarbonate $Ba_2Cu_{1.2}(CO_3)_{0.8}O_{2.4}$ [27] with the (Ba:Cu) 5:3 ratio contains much more carbon (20 at%), it has the tetragonal structure characteristic of similar oxycarbonates. Oxycarbonates, where barium is partially substituted for calcium or strontium, may contain up to 25 at% carbon. The alkaline metal–copper ratio in these oxycarbonates is in the range of 2–2.5. Barium-rich oxycarbonates can be derivative of barium–copper oxides existing in the barium-rich part of the $BaO–CuO_x$ system.

Acknowledgments

This study is supported by the Russian Foundation for Basic Research (Project No. 10-08-00475).

References

[1] K.G. Frase, D.R. Clarke, Adv. Ceram. Mater. 2 (1987) 295.
[2] F. Abbattista, M. Vallino, C. Brisi, M. Lucco-Borlera, Mater. Res. Bull. 23 (1988) 1509.
[3] D.M. De Leeuw, C.A.H.A. Mutsaers, C. Langereis, H.C.A. Smooreneburg, P.J. Rommes, Physica C 152 (1988) 39.
[4] W.K. Wong-Ng, K.L. Davis, R.S. Roth, J. Am. Ceram. Soc. 71 (1988) 64.
[5] S.F. Pashin, E.V. Antipov, L.M. Kovba, Ya.A. Skolis, Superconduct.: Phys. Chem. Eng. 2 (1989) 102.
[6] W. Zhang, K. Osamura, Jpn. J. Appl. Phys. 29 (1990) L1092.
[7] W. Zhang, K. Osamura, S. Ochiai, J. Am. Ceram. Soc. 73 (1990) 1958.
[8] M. Arjomand, D.J. Machin, J. Chem. Soc. Dalton. N4 (1975) 1061.
[9] H.N. Migeon, F. Jeannot, M. Zanne, J. Aubry, Revue de Chimie minérale 13 (1976) 440.
[10] R. Kipka, Hk. Müller-Buschbaur, Z. Naturforsch. 32b (1977) 121.
[11] L.A. Klinkova, I.V. Soikina, I.I. Zver'kova, S.A. Zver'kov, N.I. Ganovich, S.A. Shevchenko, Inorg. Mater. 25 (1989) 2033.
[12] E.F. Paulus, G. Miehe, H. Fuess, I. Yehia, U. Löchner, J. Solid State Chem. 90 (1991) 17.
[13] A.A. Zhokhov, Zh.D. Sokolovkaya, G.K. Baranova, Superconduct.: Phys. Chem. Eng. 3 (1990) 2799.
[14] K. Boroviec, J. Przyluski, K. Kolbreska, Eur. J. Solid State Inorg. Chem. 27 (1990) 333.
[15] J. Šesták, J. Kamarád, P. Holba, A. Tříska, E. Pollert, M. Nevřiva, Thermochim. Acta 174 (1991) 99.
[16] G.F. Voronin, S.A. Degterov, J. Solid State Chem. 110 (1994) 50.
[17] T.B. Lindemer, E.D. Specht, Physica C 255 (1995) 81.
[18] The reference book on diagrams of refractory oxide systems, Institute of silicates chemistry, St. Petersburg, 1997.
[19] L.A. Klinkova, V.I. Nikolaichik, N.V. Barkovskii, V.K. Fedotov, J. Solid State Chem. 146 (1999) 439.
[20] D. Harris, T.A. Hewston, J. Solid State Chem. 69 (1987) 182.
[21] E. Dubler, P. Korber, H.R. Oswald, Acta Cryst. B 29 (1973) 1929.
[22] JCPDS, No. 25-0075.
[23] JCPDS, No. 41-0164.
[24] Yu.Ya. Skolis, M.L. Kovba, Russ, J. Phys. Chem. 74 (2000) 2055.
[25] K. Peitola, M. Karppinen, H. Rundlöf, R. Tellgren, H. Yamauchi, L. Niinistö, J. Mater. Chem. 9 (1999) 2599.
[26] M.A.G. Aranda, J.P. Attfield, Angew. Chem. 105 (1993) 1511.
[27] G.B. Calestani, F.C. Matacotta, A. Migliori, P. Nozar, L. Righi, K.A. Thomas, Physica C 261 (1996) 38.
[28] C. Chaillout, Q. Huang, R.J. Cava, J. Chenavas, A. Santoro, P. Bordet, J.L. Hodeau, J.J. Krajewski, J.P. Levy, M. Marezio, W.F. Peck Jr., Physica C 195 (1992) 335.
[29] C. Greaves, P.R. Slater, J. Mater. Chem. 1 (1991) 17.
[30] M. Kikuchi, F. Izumi, M. Kikuchi, E. Ohshima, Y. Morii, Y. Shimojo, Y. Syono, Physica C 247 (1995) 183.
[31] K. Muraleedharan, C.V. Tomy, S.K. Malik, R. Prasad, N.C. Soni, Solid State Commun 68 (1988) 227.
[32] L.A. Klinkova, V.I. Nikolaichik, N.V. Barkovskii, V.K. Fedotov, Physica C 470 (2010) 2067.